ISSN 1063-7834, Physics of the Solid State, 2012, Vol. 54, No. 2, pp. 261–266. © Pleiades Publishing, Ltd., 2012.
Original Russian Text © S.V. Ovsyannikov, Yu.A. Grigor'eva, G.V. Vorontsov, L.N. Luk'yanova, V.A. Kutasov, V.V. Shchennikov, 2012, published in Fizika Tverdogo Tela, 2012, Vol. 54, No. 2, pp. 246–251.

SEMICONDUCTORS

Thermoelectric Properties of p-$Bi_{2-x}Sb_xTe_3$ Solid Solutions under Pressure

S. V. Ovsyannikov[a, *], Yu. A. Grigor'eva[a], G. V. Vorontsov[a], L. N. Luk'yanova[b, **], V. A. Kutasov[b], and V. V. Shchennikov[a]

[a] *Institute of Metal Physics, Ural Branch of the Russian Academy of Sciences, ul. Sofii Kovalevskoi 18, Yekaterinburg, 620990 Russia*
** e-mail: vladimir.v@imp.uran.ru*
[b] *Ioffe Physical-Technical Institute, Russian Academy of Sciences, Politekhnicheskaya ul. 26, St. Petersburg, 194021 Russia*
*** e-mail: lidia.lukyanova@mail.ioffe.ru*

Received July 6, 2011

Abstract—This paper reports on a study of the Seebeck coefficient and power factor κ of p-$Bi_{2-x}Sb_xTe_3$ solid solutions with different contents of antimony atoms in the bismuth sublattice for $x = 0$, 1.4, 1.5, and 1.6 under variation of pressure of up to 15 GPa. The magnitude of κ has been found to grow nonmonotonically within the pressure region of 2–4 GPa. The effective mass of the density of states m/m_0 and the mobility μ_0 have been calculated with due account of degeneracy within the parabolic model of the energy spectrum assuming isotropic charge carrier scattering. It has been shown that application of pressure brings about a decrease of the effective mass m/m_0 and an increase of carrier mobility. The power factor κ of the p-$Bi_{0.6}Sb_{1.4}Te_3$ composition exhibits at the pressure $P \approx 4$ GPa the largest increase of the power factor κ as a result of a weak decrease of the effective mass m/m_0 and an increase of carrier mobility as compared to the other solid solution compositions. The specific feature of the variation of the power factor κ with a change of the pressure in bismuth telluride near $P \approx 3$ GPa, which is accompanied by formation of a knee in the m/m_0 vs. P dependence, can be assigned to an electronic topological transition.

DOI: 10.1134/S1063783412020254

1. INTRODUCTION

A major problem in studies of thermoelectric (TE) materials is the search for ways aimed at improving their TE parameters, namely, the power factor $\kappa = S^2/\rho$ and the figure-of-merit $ZT = TS^2/(\rho\lambda)$, where S is the Seebeck coefficient, ρ is the electrical resistivity, λ is the thermal conductivity, and T is the temperature.

Bismuth telluride-based compounds Bi_2Te_3 are among the best known materials employed in high-efficiency TE modules. It has recently been demonstrated that combining synthesis with doping at a high pressure may improve noticeably the κ and ZT parameters in these compounds due to the resistivity dropping even at a comparatively small decrease of the Seebeck coefficient [1–3]. One has succeeded in obtaining, in the binary compound Bi_2Te_3 with modest starting thermoelectric parameters, a rise of the Seebeck coefficient under pressure accompanied by a substantial increase of the power factor [4]. Similar studies were conducted on other Bi_2Te_3-based materials as well (see [5]).

The purpose of this work was to study the behavior of the Seebeck coefficient and of the resistivity under pressure varied up to 15 GPa in the p-$Bi_{2-x}Sb_xTe_3$ solid solutions ($x = 0$, 1.4, 1.5, and 1.6) featuring high starting values of the TE parameters at normal pressure [6].

2. SAMPLE PREPARATION AND EXPERIMENTAL TECHNIQUE

Samples of the p-$Bi_{2-x}Sb_xTe_3$ solid solutions intended for high-pressure studies were cut from textured ingots obtained by vertical zone leveling. The ingots consisted of compacted single-crystal grains with (0001) cleavage planes oriented along the growth axis, which was perpendicular to the threefold axis C_3.

The pressure was produced by means of anvils of two types, one of them being Bridgman-type with an operating diameter $d \sim 0.6$ mm fabricated of artificial diamonds (Fig. 1a), and the other made of tungsten carbide with an operating diameter of the central hemispherical anvils $d \sim 1$ mm (Fig. 1b). In both chambers, the samples (~200 × 200 × 30 and ~200 × 200 × 250 μm^3, respectively) were sandwiched in spacers of lithographic limestone [4].

The pressure was measured with an error of ~10% with the use of a calibration curve derived for a number of materials (Be, PbS, PbSe, CdSe) which undergo phase transitions under known pressures. The force

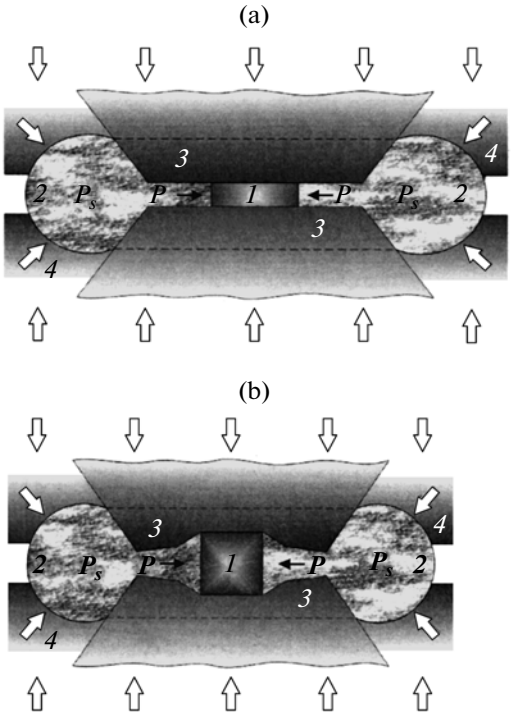

Fig. 1. Sample positioned in the high-pressure chamber: (a) diamond chamber, (b) hard-alloy chamber, (*1*) sample, (*2*) spacer of lithographic limestone serving for transmission of the pressure of the medium, (*3*) inserts of artificial diamonds (anvils), and (*4*) supporting matrices of hard alloys. The ring-shaped thickening of spacer *2* exerts supporting pressure P_s (up to 10 GPa) at the anvil edges. The high hydrostatic pressure P is generated in the central part of the chamber.

applied was measured with a digital dynamometer based on strain sensors [7–9]. The measurements were conducted on two automated high-pressure plants [4, 7–9].

The anvils exhibit a high electrical conductivity and were used as leads from the sample, as well as a heater and a cooler. The temperature difference in a sample (ΔT) in the sample was measured between the upper and the lower anvils, with thermocouples connected to the corresponding fixed points. The calculation of the temperature distribution in the "anvil-spacer-sample" system is described in [7, 8, 10, 11].

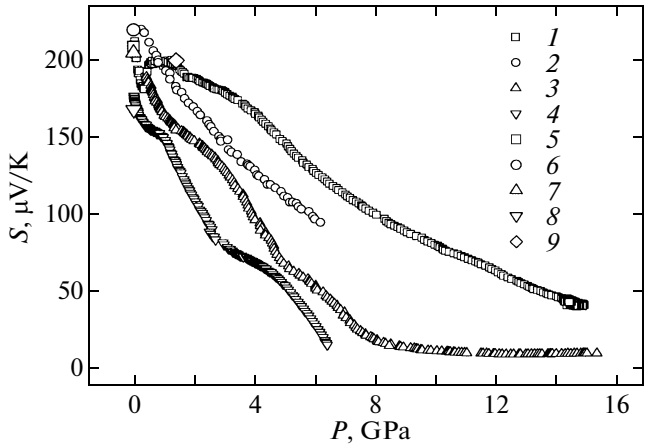

Fig. 2. Seebeck coefficient S plotted vs. pressure in the $Bi_{2-x}Sb_xTe_3$ solid solutions. x: (*1*) 1.4 (no. 7), (*2*) 1.5 (no. 8), (*3*) 1.6 (no. 6), and (*4*) 0 (no. 10).

The Seebeck coefficient was measured in three operating modes: at a fixed temperature difference ΔT and continuous variation of pressure; at a fixed pressure and gradual variation of temperature difference ΔT; and at simultaneous variation of P and ΔT. The three methods produced equal results. The resistivity ρ was measured by the double-contact method with an error of ~5%, the error of Seebeck coefficient measurement was ~10%.

3. POWER FACTOR

The Seebeck coefficient and the electrical resistivity of the p-$Bi_{2-x}Sb_xTe_3$ solid solutions with $x = 0$, 1.4, 1.5, 1.6 fell off with increasing pressure (Figs. 2, 3). The initial values of the Seebeck coefficient coincided, within experimental error, with the data obtained under normal pressure on large textured samples made up of single-crystal grains. The sample characteristics are listed in the table. At a high pressure, BiSbTe alloys undergo structural phase transitions [11] visualized on Seebeck coefficient curves (for instance, for the sample with $x = 1.6$, above ~6 GPa in Fig. 2).

The variation of the power factor on pressure $\kappa(P)$ was derived from the data obtained on the Seebeck coefficient and electrical resistivity: $\kappa = S^2/\rho$ (Figs. 3, 4). Despite the decrease of the Seebeck coefficient and

Experimental and calculated characteristics of the studied $Bi_{2-x}Sb_xTe_3$ solid solutions

Sample no.	Composition	S, μV K^{-1}	σ, Ω^{-1} cm^{-1}	κ, 10^{-6} W cm^{-1} K^{-2}	μ_0, cm^2 V^{-1} s^{-1}	m/m_0
7	$Bi_{0.6}Sb_{1.4}Te_3$	209	998	43	262	1.60
8	$Bi_{0.5}Sb_{1.5}Te_3$	220	1037	50	277	1.72
6	$Bi_{0.4}Sb_{1.6}Te_3$	205	1216	51	336	1.73
10	Bi_2Te_3	165	1400	38	268	1.50

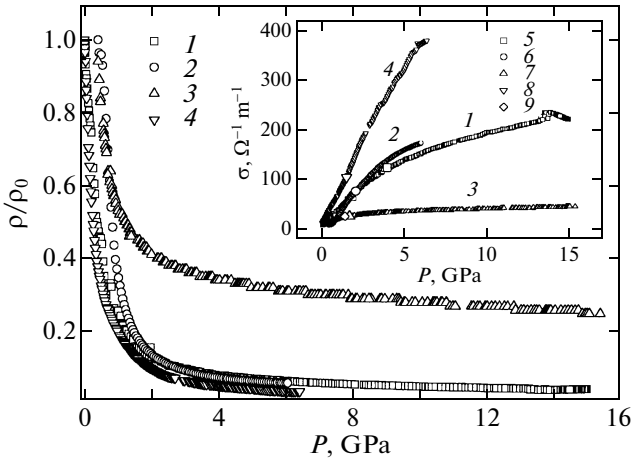

Fig. 3. Relative electrical resistivity ρ/ρ_0 plotted vs. pressure in the $Bi_{2-x}Sb_xTe_3$ solid solutions. *x*: (*1*) 1.4 (no. 7), (*2*) 1.5 (no. 8), (*3*) 1.6 (no. 6), and (*4*) 0 (no. 10). Inset to Fig. 3 presents the electrical conductivity σ plotted vs. pressure in the $Bi_{2-x}Sb_xTe_3$ solid solutions. *x*: (*1*) 1.4 (no. 7), (*2*) 1.5 (no. 8), (*3*) 1.6 (no. 6), and (*4*) 0 (no. 10). (*5*–*8*) Electrical conductivities σ at which the Seebeck coefficient reaches maximum values in samples nos. 7, 8, 6, and 10, respectively, (*9*) [12].

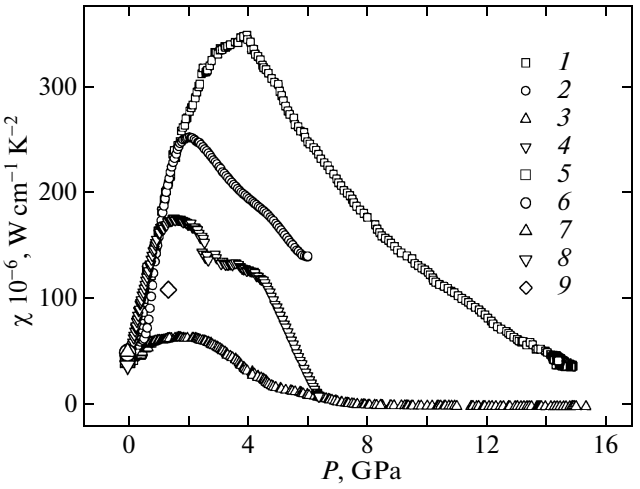

Fig. 4. Dependences of the power factor κ on pressure in the $Bi_{2-x}Sb_xTe_3$ solid solutions. *x*: (*1*) 1.4 (no. 7), (*2*) 1.5 (no. 8), (*3*) 1.6 (no. 6), and (*4*) 0 (no. 10). Power factor κ at normal pressure: (*5*) no. 7, (*6*) no. 8, (*7*) no. 6, (*8*) no. 10, and (*9*) [12].

resistivity under pressure, the power factor exhibits a nonmonotonic behavior featuring maxima in the 2–4-GPa region. In this region, the maximum value of the power factor was obtained for the $x = 1.4$ composition (Fig. 4, curve *1*). Significantly, in this study one measured actually the relative variation of the electrical resistivity, and the results were found to be slightly different for the hard alloy and the diamond chambers because of the high-pressure cells and the samples differing in shape (Figs. 1 and 3).

Sample no. 7 with a smaller concentration of substituted atoms on the Bi sublattice exhibited at $x = 1.4$ weakening of the $S(P)$ dependence; combined with the decrease of electrical resistivity (growth of electrical conductivity), this factor brought about the largest increase of the power factor as compared to the other samples (curves *1* in Figs. 2–4). The data amassed for the Seebeck coefficient, electrical conductivity and power factor in the samples under study are consistent with the results obtained for p-$Bi_{2-x}Sb_xTe_3$ ($x = 1.5$) under hydrostatic pressure of up to 1.5 GPa [12] (Figs. 2–4).

The Bi_2Te_3 sample (no. 10) reveals a change in the dependence of the power factor κ on pressure P around 3 GPa (curve *4*, Fig. 4).

4. EFFECTIVE MASS AND MOBILITY

Studies of the Seebeck coefficient S and of the electrical conductivity σ performed in the high-pressure domain on samples of the p-$Bi_{2-x}Sb_xTe_3$ solid solutions with different concentrations of antimony atoms on the bismuth sublattice offer a possibility of calculating for a one-band parabolic model of the energy spectrum with isotropic carrier scattering the effective density-of-states mass m/m_0 and mobility μ after accounting for carrier degeneracy.

Subsequent calculations of m/m_0 and μ were conducted allowing for the change of the scattering mechanism with composition and hole concentration in the solid solution by introducing an effective carrier scattering parameter r_{eff}.

The values of r_{eff} and of the reduced Fermi level η were derived by solving coupled equations for the Seebeck coefficient $S(r, \eta)$ and degeneracy parameter $\beta_d(r, \eta)$ which accounts for scattering in solid solutions. This was done by invoking the results obtained in studies of the thermoelectric and galvanomagnetic properties of Bi_2Te_3-based p-type solid solutions [13, 14].

In the materials discussed here, the acoustic mechanism of carrier scattering with the parameter $r = -0.5$ is the major process to take into account. The deviations from the value of -0.5 obtained in the calculations should be assigned to atomic substitutions on the Bi sublattice and variations in the hole concentration that affect the scattering processes.

For samples nos. 6–8 with $x = 1.4$, 1.5, and 1.6, $r_{\text{eff}} \approx -0.65$, and for sample no. 10 ($x = 0$) $r_{\text{eff}} \approx -0.75$. These values of r_{eff} are consistent with the results obtained in studies of Bi_2Te_3-based materials [15, 16].

The dependences of the Seebeck coefficient on reduced Fermi level, $S(\eta)$, and carrier concentration, $S(p)$, which are needed for calculation of the effective mass m/m_0 and mobility μ_0 were derived [13, 14] from

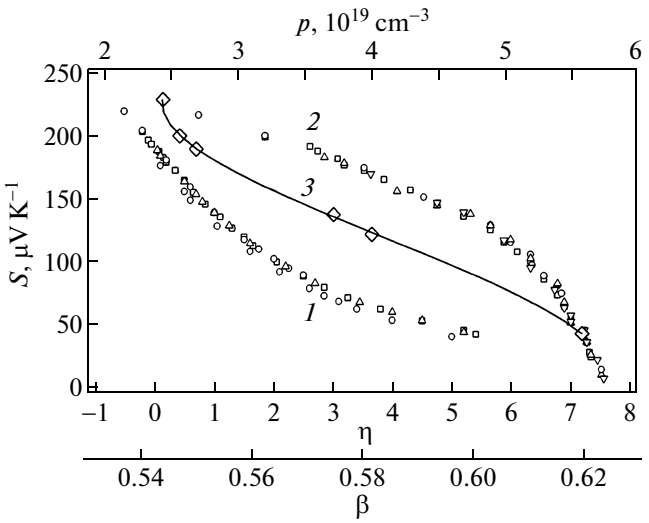

Fig. 5. Dependences of (*1*, *2*) the Seebeck coefficient S on the (*1*) reduced Fermi level η and (*2*) hole concentration p, and (*3*) the degeneracy parameter β_d on the Seebeck coefficient S in the p-$Bi_{2-x}Sb_xTe_3$ solid solutions.

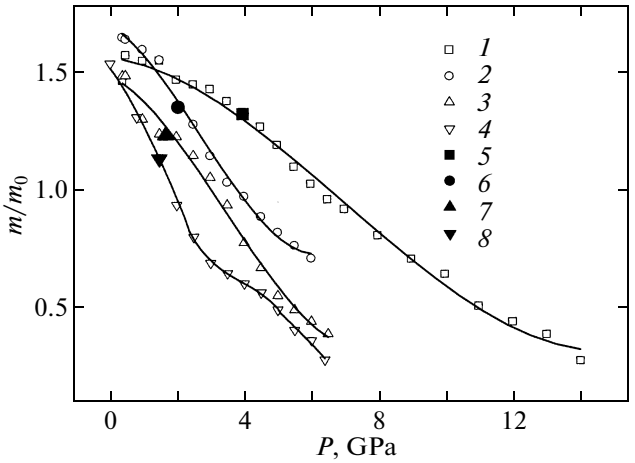

Fig. 6. Effective density-of-states mass m/m_0 plotted vs. pressure for $Bi_{2-x}Sb_xTe_3$ solid solutions. x: (*1*) 1.4, (*2*) 1.5, (*3*) 1.6, and (*4*) 0. (*5*–*8*) Effective masses m/m_0 at which the power factor reaches maximum values in samples nos. 7, 8, 6, and 10, respectively.

the studies of thermoelectric and galvanomagnetic properties in p-$Bi_{2-x}Sb_xTe_3$ solid solutions (Fig. 5).

The solid-solution samples under study are partially degenerate, a conclusion borne out from the behavior of $S(\eta)$ and $\beta_d(S)$ (Fig. 5) and studies of optical absorption at the fundamental band edge in p-type Bi_2Te_3-based solid solutions at close hole concentrations [17].

As pressure P increases, the effective mass m/m_0 decreases, as does the Seebeck coefficient (Figs. 2 and 6). Increase of x in the solid solutions brings about a sharper decrease of the effective mass under pressure. The value of m/m_0 in Bi_2Te_3 is smaller than that in the solid solutions (curve *4* in Fig. 6), both at normal pressure (see table) and at higher P (Fig. 6).

The m/m_0 vs. P graph obtained for the p-Bi_2Te_3 sample passes through a sharp bend close to the pressure ($P \approx 3$ GPa) at which a feature appears in the variation of the power factor κ with pressure (curves *4* in Figs. 4 and 6). The variation of the behavior of κ and m/m_0 in this sample with pressure at $P \approx 3$ GPa may be assigned to an electronic topological transition. The existence of a topological transition in bismuth telluride was supported by high-precision diffraction studies of the lattice constants a and c [18]. Despite a monotonic falloff of a and c in bismuth telluride with increasing pressure, at $P \approx 3$ GPa one observed a sharp change of the elasticity modulus and of its derivative in atomic layers, an effect associated with the change of lattice constant a, which was attributed [18] to an electronic topological transition.

The possibility of existence of a topological transition in p-Bi_2Te_3 is corroborated also by studies of the Seebeck coefficient and of the Shubnikov–de Haas effect under pressure [19]. As follows from these studies, in the topological transitions in p-Bi_2Te_3 which are initiated by changes in the topology of the Fermi surface, the pressure dependences of the Seebeck coefficient were observed to acquire anomalies.

In the composition with a smaller $x = 1.4$, which exhibited a pronounced increase of the power factor, the $m/m_0(P)$ dependence was found to be weaker than that observed in other compositions (curves *1*, Figs. 2 and 6). The slopes of the $d(\ln m/m_0)/d(\ln P)$ graphs obtained for the samples under study fall off from −0.07 to −0.05 and fit qualitatively to those for p-$Bi_{2-x}Sb_xTe_3$ at $x = 1.5$ calculated in terms of the many-valley model of the energy spectrum [20].

The mobility μ_0 calculated allowing for the degeneracy, first grows with increasing pressure, to become practically constant with further rise of P in samples Nos. 6–8 of the solid solution (curves *1*–*3* in Fig. 7). In the Bi_2Te_3 sample no. 10, the mobility is higher than that in the solid solutions, despite the higher carrier concentration in this sample. The slight falloff of mobility in the Bi_2Te_3 sample observed to occur for $P > 5$ GPa may be caused by the smaller bandgap width in Bi_2Te_3, in which $E_g \approx 0.15$ eV, as compared to p-$Bi_{2-x}Sb_xTe_3$ solid solutions. The values of bandgap width obtained in studies of reflection spectra for p-$Bi_{2-x}Sb_xTe_3$ in the region of plasma effects revealed that $E_g = 0.20$–0.21 eV and depends only weakly on the solid solution composition within the $x = 1.4$–1.6 interval [21].

Because the values of the effective mass m/m_0 and of the mobility μ_0 govern the power factor in solid solutions according to the relation $\kappa \sim (m/m_0)^{3/2}\mu_0$, the pattern itself of variation of these characteristics with

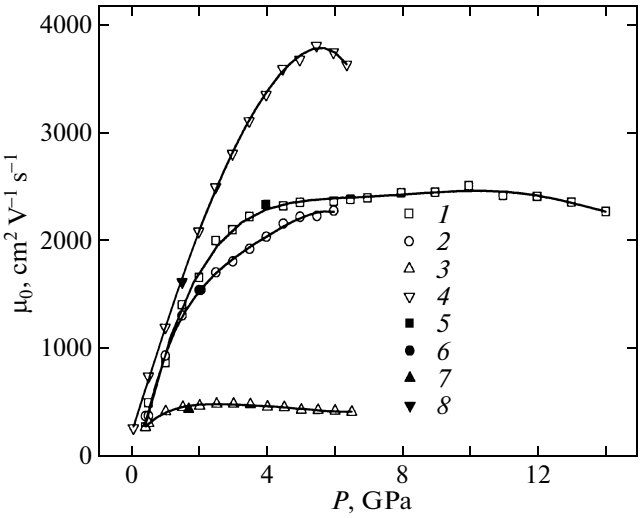

Fig. 7. Mobility μ_0 in $Bi_{2-x}Sb_xTe_3$ solid solutions plotted vs. pressure. (*1*) 1.4, (*2*) 1.5, (*3*) 1.6, and (*4*) 0. (*5–8*) Mobilities μ_0 at which the power factor reaches maximum values in samples nos. 7, 8, 6, and 10, respectively.

pressure tends to induce the most intense growth of κ in a composition with the smaller concentration of substituted atoms on the bismuth sublattice at $x = 1.4$ (curves *1*, Figs. 6 and 7) as a result of the growth of mobility and effective mass as compared to other compositions of the p-$Bi_{2-x}Sb_xTe_3$ solid solutions.

The constant-energy surface of the materials under study is usually described in terms of the many-valley model of energy spectrum consisting of six ellipsoids. The pattern of variation of the effective mass m/m_0 is governed by the ratios of the components of the effective mass tensor m_i/m_j determining the parameters of the constant-energy ellipsoids and reflects different anisotropies of the constant-energy surface in the valence band of the p-$Bi_{2-x}Sb_xTe_3$ solid solutions. The difference in the pressure-induced decrease of the m/m_0 effective mass in solid solutions of different compositions can be assigned to variation of the component ratio of the effective mass tensor m_i/m_j with concentration of Sb atoms. The sharp bend in the dependence of m/m_0 on P observed to occur in bismuth telluride at $P \approx 3$ GPa (curve *4*, Fig. 6) also suggests a pressure-induced change of the parameters of the constant-energy surface initiated by an electronic topological transition.

The results of the studies of galvanomagnetic effects occurring at normal pressure in $Bi_{2-x}Sb_xTe_3$ solid solutions which were analyzed in the context of the many-valley model of the energy spectrum assuming isotropic carrier scattering demonstrated a variation of compression of the constant-energy ellipsoids along the binary and bisectrix axes, as well as a variation of extension along the trigonal axis, depending on composition and carrier concentration [14].

Application of pressure may initiate further stretching of the axes and formation of bars connecting constant energy ellipsoids and of a closed Fermi surface. Further increase of pressure may bring about fracture of the bars, which will make the surface ellipsoidal again [22]. In the model of the energy spectrum considered here, the effect of the second valence band in the $Bi_{2-x}Sb_xTe_3$ solid solutions was disregarded. Pressure may, however, also induce changes in the parameters of this heavy valence band in solid solutions and, accordingly, produce the observed nonmonotonic dependences of the Seebeck coefficient and the power factor (Figs. 2 and 4).

5. CONCLUSIONS

Our studies of the Seebeck coefficient S and the power factor under pressure in p-$Bi_{2-x}Sb_xTe_3$ solid solutions of different compositions at $x = 0$, 1.4, 1.5, and 1.6 showed the Seebeck coefficient and electrical resistivity to decrease with increasing pressure.

The growth of the power factor $\kappa \sim (m/m_0)^{3/2}\mu_0$ revealed in the 2–4 GPa pressure interval is the result of reaching optimum relations between the effective density-of-states m/m_0 and carrier mobility μ_0 calculated for the parabolic model of the energy spectrum with isotropic scattering and with allowance for variation of the scattering mechanism in the dependence on the solid solution composition. The largest increase of the κ parameter, observed to occur at $P \approx 4$ GPa in the composition with a smaller concentration of Sb at $x = 1.4$, is accounted for by a weakening of the $m/m_0(P)$ dependence as compared to the other solid solution compositions.

The knee in the dependence of m/m_0 on P in bismuth telluride near the pressure $P \approx 3$ GPa, at which a feature appears in the dependence of the power factor κ on pressure, can be attributed to an electronic topological transition.

Carrier mobility in samples of this composition grows up to 4 GPa. The variations of the effective mass m/m_0 induced by pressure should be assigned to the decrease of the bandgap width, as well as to other features in the variation of the energy spectrum and are mediated by the parameters of the ellipsoidal constant-energy surface of the p-$Bi_{2-x}Sb_xTe_3$ solid solutions.

ACKNOWLEDGMENTS

This study was supported by the Russian Foundation for Basic Research (project nos. 10-08-00945, 10-08-00645) and the Presidium of the Russian Academy of Sciences (program no. 09-P-2-1020).

REFERENCES

1. F. J. DiSalvo, Science (Washington) **285**, 703 (1999).

2. T. M. Tritt, Science (Washington) **283**, 804 (1999).
3. R. Venkatasubramanian, E. Siivola, T. Colpitts, and B. O'Quinn, Nature (London) **413**, 597 (2001).
4. S. V. Ovsyannikov, V. V. Shchennikov, G. V. Vorontsov, A. Y. Manakov, A. Y. Likhacheva, and V. A. Kulbachinskii, J. Appl. Phys. **104**, 053713 (2008).
5. J. F. Meng, N. V. Shekar, J. V. Badding, D. Y. Chung, and M. G. Kanatzidis, J. Appl. Phys. **90** (6), 2836 (2001).
6. L. N. Luk'yanova, V. A. Kutasov, V. V. Popov, and P. P. Konstantinov, Phys. Solid State **48** (4), 647 (2006).
7. V. V. Shchennikov, S. V. Ovsyannikov, G. V. Vorontsov, and V. V. Kulbachinskii, J. Phys.: Conf. Ser. **215**, 012185 (2010).
8. S. V. Ovsyannikov and V. V. Shchennikov, in *Book of Abstracts of the 14th HPSP International Conference on High Pressure Semiconductor Physics*, Changchun, China, August 1–4, 2010, p. 36.
9. M. K. Jacobsen, R. S. Kumar, A. L. Cornelius, S. V. Sinogeiken, and M. F. Nicol, in *Shock Compression of Condensed Matter*, Ed. by M. Elert, M. D. Furnish, R. Cliau, N. Holmes, and J. Nguyen (American Institute of Physics, New York, 2007).
10. S. V. Ovsynnikov and V. V. Shchennikov, Chem. Mater. **22** (3), 635 (2010).
11. V. V. Shchennicov, S. V. Ovsyannikov, and A. Y. Manakov, J. Phys. Chem. Solids **71** (8), 1168 (2010).
12. A. A. Averkin, B. M. Gol'tsman, V. A. Kutasov, A. R. Regel', Yu. Z. Sanfirov, L. S. Stil'bans, and Zh. Zh. Zhaparov, in *Proceedings of the All-Union Workshop on Deformation and Dimensional Effects in Thermoelectric Materials and Films, Technology and Application of Films "Thermoelectric Materials and Films,"* Ioffe Physical-Technical Institute, Academy of Sciences of the USSR, Leningrad, 1976, p. 4.
13. L. N. Luk'yanova, V. A. Kutasov, V. V. Popov, and P. P. Konstantinov, Phys. Solid State **46** (8), 1404 (2004).
14. L. N. Luk'yanova, V. A. Kutasov, V. V. Popov, and P. P. Konstantinov, Phys. Solid State **52** (8), 1599 (2010).
15. H. Kaibe, Y. Tanaka, M. Sakata, and I. Nishida, J. Phys. Chem. Solids **50**, 945 (1989).
16. V. A. Kulbachinskii, A. V. G. Kytin, and P. M. Tarasov, in *Proceedings of the XXV International Conference on Thermoelectrics*, IEEE, Austria, Vienna, 2006, p. 496.
17. A. N. Veis, L. N. Luk'yanova, and V. A. Kutasov, in *Proceedings of the XII International Workshop "Thermoelectrics and Their Applications,"* St. Petersburg, 2010, p. 133.
18. A. Polian and M. Gauthier, Phys. Rev. B: Condens. Matter **83**, 113106 (2011).
19. E. S. Itskevich, L. M. Kashirskaya, and V. F. Kraidenov, Semiconductors **31** (3), 276 (1997).
20. A. A. Averkin, O. S. Gryaznov, Yu. Z. Sanfirov, and V. E. Seleznev, in *Proceedings of the All-Union Workshop "Thermoelectric Materials and Films"*, Ioffe Physical-Technical Institute, Academy of Sciences of the USSR, Leningrad, 1976, p. 8.
21. N. P. Stepanov and A. A. Kalashnikov, Semiconductors **44** (9), 1129 (2010).
22. V. B. Ansin, M. S. Bresler, I. I. Farbshtein, E. S. Itskevich, Yu. V. Kosichkin, V. A. Sukhoparov, A. S. Telepnev, and V. G. Veselago, Phys. Status Solidi B **48**, 531 (1977).

Translated by G. Skrebtsov